Journal of the Geological Society, London, Vol. **170**, 2013, pp. 175–184. doi: 10.1144/jgs2012-066.

U–Pb zircon ages of Late Cretaceous Nain–Dehshir ophiolites, central Iran

HADI SHAFAII MOGHADAM[1*], FERNANDO CORFU[2] & ROBERT J. STERN[3]

[1]*School of Earth Sciences, Damghan University, Damghan, Iran*

[2]*Department of Geosciences, University of Oslo, Blindern, N-0316 Oslo, Norway*

[3]*Department of Geosciences, University of Texas at Dallas, Richardson, TX75083-0688, USA*

**Corresponding author (e-mail:hadishafaii@du.ac.ir)*

Abstract: Late Cretaceous Zagros ophiolites are part of the *c*. 3000 km long Late Cretaceous Ophiolite Belt of SW Asia including the Troodos (Cyprus), eastern Mediterranean (Turkey, Syria), Zagros (Iran) and Semail ophiolites (Oman). This ophiolite belt represents a magmatic forearc that formed when subduction of the Neotethys began along the SW margin of Eurasia. Geochronological data for Zagros ophiolites are limited to a few K–Ar and ^{40}Ar–^{39}Ar ages. New thermal ionization mass spectrometry U–Pb zircon ages indicate that the Nain and Dehshir ophiolites of central Iran formed *c*. 101–103 Ma, with Nain (102.9 ± 0.3 Ma) being *c*. 1 Ma older than Dehshir (100.9 ± 0.2 Ma; 100.4 ± 0.1 Ma), and that these ophiolites were emplaced almost immediately after formation (Nain emplacement 101.2 ± 0.2 Ma; Dehshir emplacement 99.0 ± 1.1 Ma). These formation ages are significantly older than the 98–90 Ma U–Pb zircon ages of other Late Cretaceous ophiolites in this belt such as the Kizildag (Turkey), Semail (Oman) and Troodos ophiolites (Cyprus). If the subduction initiation model applies to this ophiolite belt, it suggests that subduction initiation began near the Zagros margin and propagated at *c*. 7 cm a^{-1} to the east (Semail) and *c*. 15 cm a^{-1} to the west (Troodos).

Supplementary materials: Simplified geological maps of the Nain and Dehshir ophiolites, showing sample locations, are available at www.geolsoc.org.uk/SUP18554.

Ever since ophiolites were recognized as oceanic lithosphere fragments exposed on land, their formation has been debated. It is still controversial whether specific ophiolites are created at a mid-oceanic ridge or at a convergent plate margin, and, if at the latter, whether it was a forearc (protoarc) or back-arc basin (Miyashiro 1975; Coleman 1984). Indeed, it has been found that many ophiolites, including Neotethyan ophiolites in the Eastern Mediterranean region as well as the Indus–Yarlung Zangbo ophiolites in southern Tibet, show geochemical signatures that are typical of modern suprasubduction-zone environments (Elthon 1991; Pearce 2003; Hebert *et al*. 2012).

As a result of studying Izu–Bonin–Mariana forearc crust (Reagan *et al*. 2010; Ishizuka *et al*. 2011) and from comparing this with the magma stratigraphy in well-preserved ophiolites (Whattam & Stern 2011) we are starting to better understand the relationship between ophiolites and the formation of new subduction zones. The process of subduction initiation and its relationship with ophiolite formation remain controversial, although it seems likely that the gravitational instability of old oceanic plates provides the primary force for subduction initiation (Vlaar & Wortel 1976; Davies 1999; Stern 2004; Gerya 2011).

One way to start a new subduction zone is via collapse of dense lithosphere on one side of a transform or fracture zone leading to asthenospheric upwelling over the subsiding slab, resulting in sea-floor spreading to form a proto-forearc (Leng & Gurnis 2011), which ultimately may be emplaced as ophiolite. Thus, a good approach for studying subduction initiation is to study well-preserved ophiolites (Stern *et al*. 2012), which generally record these processes. This model was recently applied to Late Cretaceous ophiolites of Iran (Zagros ophiolites; Fig. 1) by Shafaii Moghadam *et al*. (2010) and Shafaii Moghadam & Stern (2011). Zagros ophiolites are part of one of the most extensive and best-studied ophiolite belts in the world, which can be traced for more than 3000 km along the SW margin of Eurasia, from Cyprus through SE Turkey, NW Syria, NE Iraq, SW Iran and northern Oman (Fig. 1). For the sake of brevity, we call this the Late Cretaceous Ophiolite Belt of SW Asia (LCOBSA). LCOBSA ophiolites are obducted onto the Arabian passive margin (e.g. Kizildag, Troodos, Oman, Kermanshah and Neyriz ophiolites) and/or are accreted against the Tauride–central Iranian block (e.g. Guleman and Goksun ophiolites of Turkey and Nain–Baft ophiolites of Iran) (e.g. Yilmaz 1993; Yilmaz *et al*. 1993; Parlak *et al*. 2004; Bagci *et al*. 2005).

Our understanding of the tectonic origin of LCOBSA ophiolites is advancing rapidly. Recent geochemical and geochronological studies in the LCOBSA (including Zagros ophiolites) show a temporal evolution in the volcanic sequence from mid-ocean ridge basalt (MORB)-like tholeiitic to calc-alkalic and boninitic suites (e.g. Shervais 2001; Dilek & Flower 2003; Dilek & Thy 2009; Parlak *et al*. 2009; Whattam & Stern 2011; and references therein). Troodos is somewhat different (its lower lavas have calc-alkaline affinities) perhaps because it formed at the edge of the new convergent margin (Pearce & Robinson 2010). With this exception, LCOBSA magma stratigraphy is similar to that documented for the Izu–Bonin–Mariana convergent margin, where forearc crust formed via sea-floor spreading during subduction initiation (Reagan *et al*. 2010; Ishizuka *et al*. 2011).

The interpretation that the LCOBSA reflects a subduction initiation event is controversial and needs further testing and refinement. One of the greatest challenges concerns understanding how long it took for subduction initiation to occur, where this instability first formed, and how the collapsing margin evolved. Because subduction initiation is likely to begin at one site and then propagate along strike, there should be an age progression. Understanding the age of ophiolites along the LCOBSA is thus a critical test of the general idea; this model predicts an age progression of ophiolite formation along the collapsing margin. For this reason, Zagros ophiolite ages are the 'critical missing link' in understanding the LCOBSA. The purpose of the present study is to contribute to understanding LCOBSA evolution by

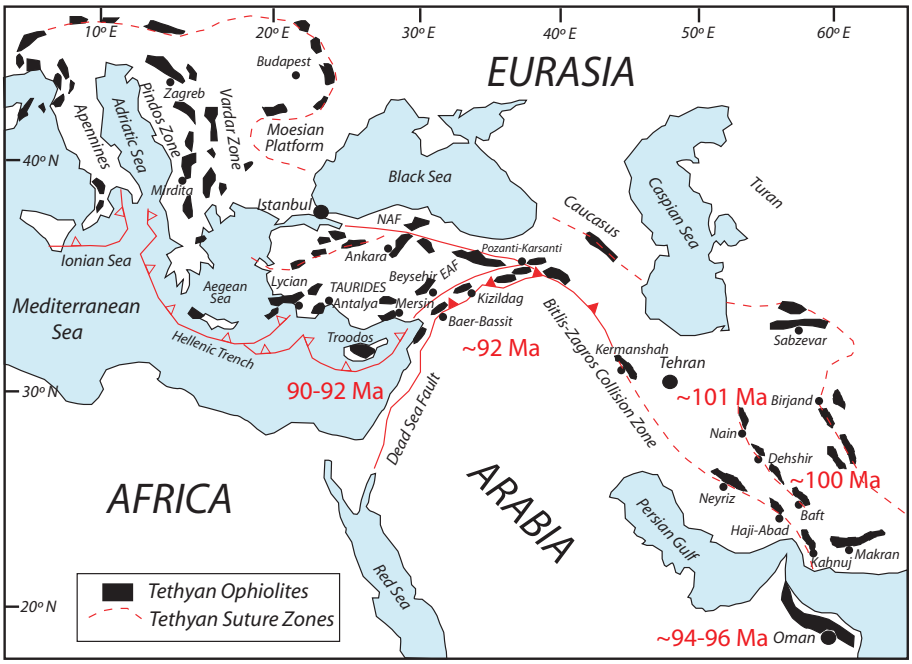

Fig. 1. Simplified tectonic map of the eastern Mediterranean–Zagros region showing the distribution of Neotethyan ophiolites and suture zones (modified after Dilek *et al*. 2007). The U–Pb zircon ages for Troodos ophiolite trondhjemites and gabbro are from Mukasa & Ludden (1987), for Kizildag from Dilek & Thy (2009), for Oman from Warren *et al*. (2005) and Goodenough *et al*. (2010), and for the Nain–Dehshir ophiolites are from this study. NAF, North Anatolian Fault; EAF, East Anatolian Fault.

reporting new thermal ionization mass spectrometry (TIMS) U–Pb zircon ages of the Nain and Dehshir ophiolites. These are the first U–Pb zircon ages reported for the Zagros ophiolites of Iran.

Geological setting

Late Cretaceous ophiolites along the Bitlis–Zagros suture zone are remnants of Neotethys oceanic lithosphere, which separated Gondwanaland from Eurasia. LCOBSA fragments in Cyprus (Troodos), Turkey (Kizildag, Goksun, Elazig), Syria (Baer–Bassit), Iran (Zagros ophiolites) and Oman (Semail) have suprasubduction-zone geochemical affinities (e.g. Alabaster *et al*. 1982; Hébert & Laurent 1990; Sengor 1990; Lytwyn & Casey 1993; Parlak *et al*. 1996, 2000, 2009; Yaliniz *et al*. 1996; Floyd *et al*. 1998; Robertson 2002; Godard *et al*. 2003, 2006; Bagci *et al*. 2005, 2006, 2008; Warren *et al*. 2005; Babaie *et al*. 2006; Goodenough *et al*. 2010; Shafaii Moghadam *et al*. 2010; Shafaii Moghadam & Stern 2011). LCOBSA suprasubduction-zone affinities are also indicated by mineral compositions of gabbros and mantle peridotites (e.g. Umino *et al*. 1990; Bagci *et al*. 2005; Arai *et al*. 2006; Yamasaki *et al*. 2006; Python *et al*. 2008; Bagci & Parlak 2009; Shafaii Moghadam & Stern 2011; Uysal *et al*. 2012). LCOBSA ophiolite lavas show geochemical transitions up-sequence, from MORB-like to more island arc or boninite-like compositions, consistent with formation during subduction initiation (Whattam & Stern 2011).

Zagros ophiolites constitute the central parts of the LCOBSA and define two parallel belts along the NE flank of the Zagros fold–thrust belt in Iran (Fig. 2; Sengor 1990; Robertson 1998, 2002; Garfunkel 2006; Robertson & Mountrakis 2006; Dilek *et al*. 2007; Dilek & Furnes 2011; Shafaii Moghadam & Stern 2011). Zagros ophiolites can be subdivided into an 'Inner Belt' (Inner Zagros Ophiolite Belt) and an 'Outer Belt' (Outer Zagros Ophiolite Belt), south of the Main Zagros Thrust Fault and along the SW periphery of the Central Iranian block, respectively (Stocklin 1977; Fig. 2). The two ophiolite belts are separated by metamorphic rocks of the Sanandaj–Sirjan Zone. Several hypotheses have been proposed for the genesis and evolution of Inner Belt ophiolites (the focus of our study), including an origin as a back-arc basin (Agard *et al*. 2006; Shafaii Moghadam *et al*. 2009; Agard *et al*. 2011) or in a proto-forearc, during subduction initiation (Shafaii Moghadam *et al*. 2010; Shafaii Moghadam & Stern 2011).

Northward subduction of Neotethyan ocean floor beneath Iran generated a 50–80 km wide Andean-type magmatic belt of Cenozoic intrusive and extrusive rocks, the Urumieh–Dokhtar magmatic assemblage or arc (Fig. 2; Falcon 1974; Berberian & Berberian 1981; Berberian & King 1981; Berberian *et al*. 1982; Alavi 1994; Shahabpour 2007). This magmatic assemblage includes a thick (*c*. 4 km) pile of early calc-alkaline and later shoshonitic as well as alkaline rocks (Alavi 2007).

Nain ophiolite

The Nain ophiolite lies in the northwestern part of the Inner Belt, where it covers about 600 km^2. This ophiolite was first described by Davoudzadeh (1972) as a Late Cretaceous–Early Eocene coloured mélange. Recently, Rahmani *et al*. (2007) inferred a suprasubduction-zone tectonic environment for its formation, based on the composition of the sheeted dyke complex. The Nain ophiolite includes a well-preserved mantle sequence of depleted harzburgite with minor lherzolite. Pegmatite gabbros, isotropic gabbros and gabbronorites are common as small pockets (average 2 m × 3 m) within the mantle rocks. Pyroxenitic, gabbroic, gabbronoritic and doleritic dykes and sills crosscut the peridotites (Fig. 3a).

Nain ophiolitic rocks show geochemical signatures indicating a suprasubduction-zone origin, including depletion of Nb and REE relative to MORB. Shafaii Moghadam & Stern (2011) argued that these rocks formed in a proto-forearc during subduction initiation. The Nain sheeted dyke complex comprises mafic and felsic microgabbroic, gabbronoritic, doleritic and dacitic dykes with mutually intrusive contacts. These dykes intrude host amphibole gabbros or microgabbro and plagiogranite (Fig. 4b) and/or are injected into other dykes. The Nain ophiolite is stratigraphically overlain by Upper Cretaceous *Globotruncana*-bearing (Coniacian–Maastrichtian) pelagic limestones and radiolarites. Garnet amphibolites occur SW of Ahmad-Abad village, intruded by tonalitic dykes (Fig. 4a) with sheared contacts against ultramafic rocks.

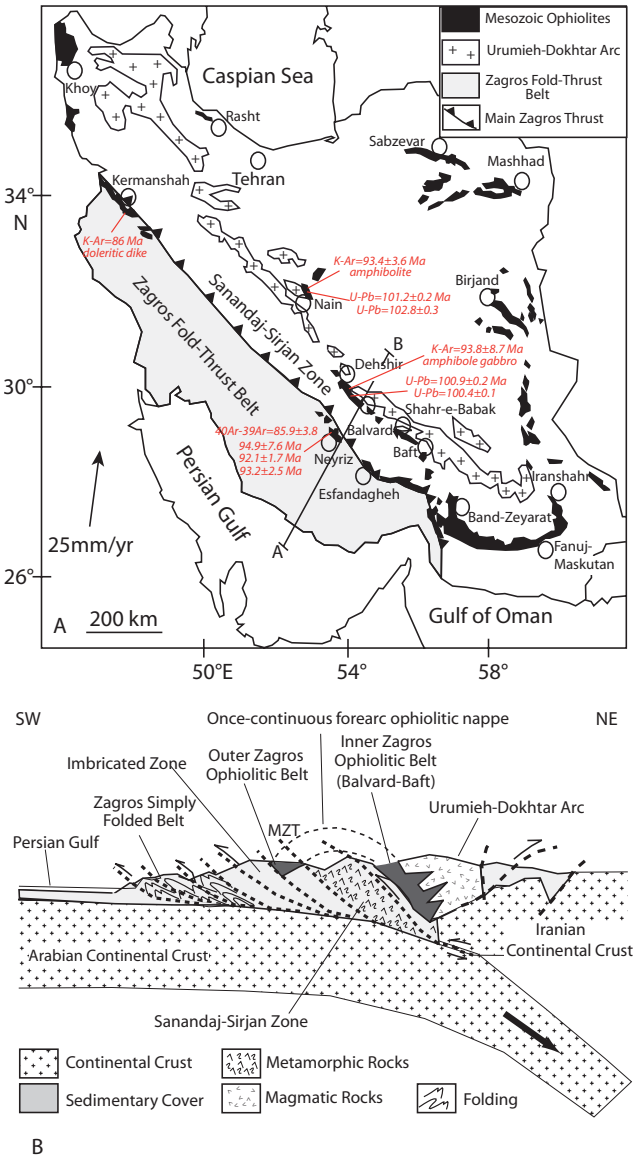

Fig. 2. Principal geological features and ophiolites of Iran. (**a**) Map showing the distribution of the inner (Nain–Dehshir–Baft–Shahr-e-Babak) and outer (Kermanshah–Neyriz–Haji–Abad) Zagros ophiolitic belts, the location of the Urumieh–Dokhtar magmatic arc (Eocene–Quaternary), and Main Zagros Thrust (MZT). (**b**) Schematic cross-section showing the relationship between outer and inner Zagros ophiolitic belts and the Zagros thrust–fold belt (after Shafaii Moghadam *et al*. 2010). U–Pb and previous K–Ar and ^{40}Ar–^{39}Ar ages are shown. K–Ar and U–Pb zircon ages for the Nain and Dehshir ophiolites are from Shafaii Moghadam *et al*. (2009) and this study, respectively; K–Ar ages for the Kermanshah ophiolites are from Delaloye & Desmons (1980), and for Neyriz ophiolites are from Lanphere & Pamic (1983), Jannessary (2003) and Babaie *et al*. (2006).

Geochemically the amphibolites have suprasubduction-zone affinities, similar to pillow lavas and isotropic gabbros; hence they may have the same protolith. Tonalitic dykes intrude only amphibolites.

Dehshir ophiolite

The Dehshir ophiolite is exposed discontinuously over *c*. 150 km^2 near the centre of the Inner Belt, about 200 km SE of the Nain ophiolite (Shafaii Moghadam *et al*. 2010). Its lava sequence is conformably capped by Turonian–Maastrichtian (93.5–65.5 Ma) *Globotruncana*-bearing pelagic limestones. The mantle sequence is represented by harzburgite with minor cumulate rocks including plagioclase lherzolite, clinopyroxenite, leucogabbro and pegmatite gabbro. Doleritic dykes and isotropic gabbros intrude the harzburgite (Fig. 3b).

The Dehshir ophiolite crustal section comprises pillowed basalts, basaltic to andesitic massive flows and a basaltic–dacitic sheeted dyke complex (Fig. 3b). Amphibole gabbros and diorites make up most of the crustal sequence (Fig. 3b). Plagiogranite occurs as dykelets injected into amphibole-bearing isotropic gabbro and diorite (Fig. 4c). Slightly metamorphosed lavas and their pyroclastic equivalents include greenschists (with island-arc tholeiitic signature). Tonalitic plugs (of Cenomanian age; see next section for U–Pb ages) intrude the greenschists (Fig. 4d). Dehshir ophiolite magmatic rocks show Nb depletions, indicating generation from a subduction-modified mantle source (Shafaii Moghadam *et al*. 2010).

Analytical methods

To constrain the timing of crystallization of Zagros ophiolites, two plagiogranitic or tonalitic samples from the Nain ophiolite and three plagiogranitic and dioritic samples from the Dehshir ophiolite were dated by the U–Pb zircon isotope dilution (ID)-TIMS technique at the University of Oslo (Table 1). The rocks were crushed in a jaw crusher and hammer mill, and the heavy minerals were concentrated using a succession of Wilfley table, free fall and high gradient magnetic separation, and methylene iodide density separation. Further selection was carried out by hand-picking under a binocular microscope and mechanical abrasion (Krogh, 1982) to remove discordant domains. Some fractions were also subjected to chemical abrasion based on the study by Mattinson (2005) but following approximately the procedure of Schoene *et al*. (2006) with an annealing stage of 3 days at 900 °C, a partial dissolution step with HF (+ HNO_3) at 194 °C overnight, and a 2 h hotplate step in 6N HCl after removal of the solution and some rinsing. The dissolution was carried out following Krogh (1973) as described by Corfu (2004) but using a mixed ^{202}Pb–^{205}Pb–^{235}U spike. The data have been corrected for ^{230}Th disequilibrium (Schärer 1984) assuming $Th/U_{magma} = 4$; this increases $^{206}Pb/^{238}U$ ages by about 0.1 Ma. Calculations were carried out with the decay constants of Jaffey *et al*. (1971) and the Isoplot program of Ludwig (2003).

Sample descriptions and results

Nain ophiolite: sample N09-21 (tonalitic dyke in amphibolite)

Tonalitic dykes cut garnet amphibolites of the basal metamorphic sole, south of the Kud-Zard village (Fig. 4a). Tonalitic dykes mainly consist of deformed quartz and plagioclase phenocrysts. Quartz defines the stretching lineation of the rock and shows serrated margins that bulge into neighbouring crystals, suggesting grain boundary migration owing to recrystallization. Plagioclase shows deformation twins and is partially altered to sericite, calcite and epidote. This highly deformed texture indicates that dykes were injected into shear zones during ophiolite emplacement and formation of the metamorphic sole. These dykes thus date emplacement of the ophiolite rather than ophiolite igneous activity.

Garnet, muscovite and amphibole are minor minerals. The sample has very low REE contents with concave-upward pattern (Fig. 5a) and slight positive Eu anomaly. The dyke also shows negative Nb–Ti anomalies relative to normal (N)-MORB, characteristic of suprasubduction-zone magmas (Fig. 5b).

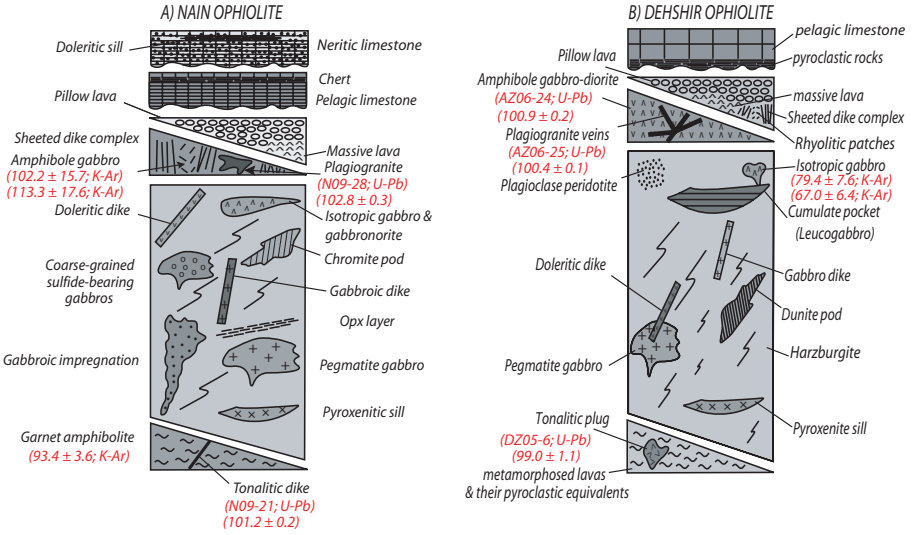

Fig. 3. Simplified lithological successions for the Nain (**a**) and Dehshir (**b**) ophiolites, showing the approximate positions (geological relations) of the dated samples.

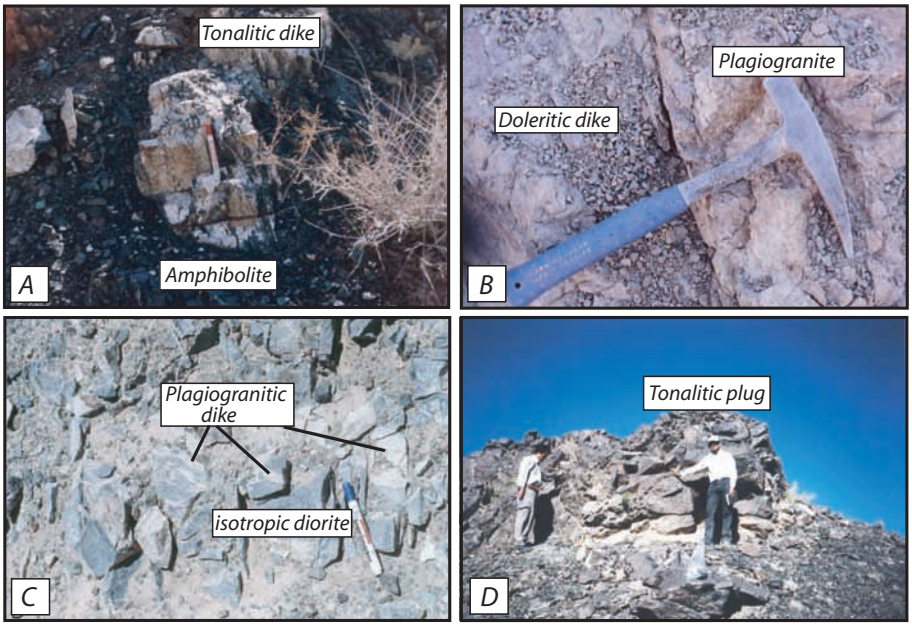

Fig. 4. Field photographs of the dated samples from the Nain and Dehshir ophiolites. (**a**) Nain ophiolite, tonalitic dyke (sample N09-21) intruding garnet amphibolite, south of Kud-Zard village. (**b**) Nain ophiolite, contact of sheeted doleritic dyke intruding plagiogranite (sample N09-28) near Ahmad-Abad village. (**c**) Dehshir ophiolite, injection of plagiogranitic dykes (sample AZ06-25) into isotropic diorites (sample AZ06-24) SW of Aziz-Abad village. (**d**) Dehshir ophiolite. Outcrop of tonalitic plug (sample DZ05-6) intruding metamorphosed lavas and pyroclastic equivalents near Zoolouzar village.

Zircon in sample N09-21 occurs as euhedral prismatic crystals (Fig. 6), mostly broken fragments. The four U–Pb analyses form two clusters (101.2±0.2 and 102.8±0.3 Ma; Table 1). The younger cluster is defined by a zircon tip and a fraction of flat prisms, whereas the older cluster includes a short prism and a fraction of several prisms (Fig. 6). The data can be interpreted in two ways: (1) the two younger analyses were affected by Pb loss and the two older analyses better reflect the age of crystallization, or (2) the two older analyses are affected by some inheritance (perhaps from Iranian continental crust) whereas the younger reflect the age of clean magmatic zircon. The second alternative is preferred because all grains were subjected to chemical abrasion, which generally removes parts affected by Pb loss in zircons of such good quality and age, and, on the other hand, because one of the zircons giving the older ages revealed some internal heterogeneity after partial dissolution, supporting the presence of an inherited core (the other fraction consistent of several grains). In our preferred interpretation, the mean $^{206}Pb/^{238}U$ age of 101.2±0.2 Ma of the two younger analyses is considered to date crystallization of the dyke (Fig. 6). The low Th/U ratio of these analyses (0.02–0.03) is common for zircon of highly evolved tonalitic magmas. These types of tonalites are not *in situ* differentiated rocks and their occurrence type, mineralogy, texture and age are consistent with derivation from partial melting of amphibolites during ophiolite emplacement. Therefore, we take this age to approximate the time of ophiolite emplacement.

Nain ophiolite: sample N09-28 (plagiogranite)

This type of plagiogranite is found mainly near the Ahmad-Abad village. It intrudes amphibole gabbros that host the sheeted dyke complex. Sheeted dyke complex dolerites intrude both amphibole gabbro and plagiogranite (Fig. 4b). These types of plagiogranite occur near the gabbro-sheeted dyke complex boundary. Plagiogranite is coarse-grained with a granular texture and is mainly composed of quartz and plagioclase with minor alkali feldspar and hornblende. Feldspars are altered to clays and sericite, with minor epidote and titanite. Chlorite is common at the expense of hornblende. The plagiogranite has a fractionated but flat REE pattern (Fig. 5a), and is enriched in large ion

Table 1. *U–Pb data for zircon from felsic plutonic rocks of the Nain and Dehshir ophiolites*

Zircon characteristics[1]	Weight[2] (μg)	U[2] (ppm)	Th/U[3]	Pbc[4] (pg)	$^{206}Pb/^{204}Pb$[5]	$^{207}Pb/^{235}U$[6]	±2σ (abs)	$^{206}Pb/^{238}U$[6]	±2σ (abs)	rho	$^{207}Pb/^{206}Pb$[6]	±2σ	$^{206}Pb/^{238}U^{6}$ (Ma)	±2σ	$^{207}Pb/^{235}U^{6}$ (Ma)	±2σ
N09-21, tonalitic dyke (Separo), Nain ophiolite (33°07'87"N, 53°02'19")																
eu tip CA [1]	9	80	0.03	1.3	587	0.1061	0.0015	0.01582	0.00004	0.46	0.04864	0.00062	101.2	0.3	102.4	1.3
eu flat prisms CA [7]	34	67	0.03	2.0	1140	0.10620	0.00085	0.01583	0.00004	0.52	0.04865	0.00034	101.3	0.3	102.5	0.8
eu short prism CA [1]	17	48	0.10	1.9	441	0.10869	0.00202	0.01610	0.00007	0.43	0.04895	0.00085	103.0	0.4	104.8	1.9
eu long prisms CA [12]	30	65	0.02	12.8	172	0.10986	0.00240	0.01619	0.00006	0.28	0.04922	0.00104	103.5	0.4	105.8	2.2
N09-28, plagiogranite (Ahmad-Abad), Nain ophiolite (32°55'93"N, 53°05'67"E)																
eu fr A [15]	13	566	0.51	1.0	7099	0.10646	0.00031	0.01605	0.00003	0.80	0.04811	0.00009	102.6	0.2	102.7	0.3
eu fr A [13]	16	594	0.55	1.1	8898	0.10655	0.00029	0.01605	0.00003	0.84	0.04814	0.00007	102.7	0.2	102.8	0.3
eu fr A [19]	28	403	0.52	1.0	11791	0.10707	0.00032	0.01612	0.00004	0.81	0.04817	0.00009	103.1	0.2	103.3	0.3
eu fr A [8]	22	411	0.48	1.1	8499	0.10682	0.00028	0.01607	0.00003	0.82	0.04820	0.00007	102.8	0.2	103.0	0.3
AZ06-25, plagiogranite (AzizAbad), Dehshir ophiolite (31°16'23"N, 53°56'43"E)																
fr (eu) A [17]	140	49	0.55	2.5	2721	0.10406	0.00038	0.01571	0.00004	0.71	0.04805	0.00012	100.5	0.2	100.5	0.3
fr (eu) A [25]	137	100	0.57	2.2	6057	0.10426	0.00037	0.01568	0.00004	0.83	0.04823	0.00010	100.3	0.2	100.7	0.3
fr (eu) A [38]	84	103	0.54	1.8	4616	0.10392	0.00037	0.01568	0.00003	0.69	0.04807	0.00012	100.3	0.2	100.4	0.3
fr (eu) A [31]	119	82	0.46	1.4	6678	0.10335	0.00029	0.01560	0.00003	0.82	0.04804	0.00008	99.8	0.2	99.9	0.3
AZ06-24, diorite (host of plagiogranite AZ06-25) (AziAbad), Dehshir ophiolite (31°16'23"N, 53°56'43"E)																
eu broken prism A [1]	2	303	0.68	2.9	224	0.10563	0.00293	0.01576	0.00011	0.43	0.04862	0.00124	100.8	0.7	102.0	2.7
eu broken prism A [1]	2	165	0.50	1.6	228	0.10423	0.00397	0.01577	0.00007	0.50	0.04793	0.00173	100.9	0.5	100.7	3.6
eu broken prism A [1]	4	207	0.50	1.2	709	0.10482	0.00127	0.01578	0.00005	0.47	0.04819	0.00053	100.9	0.3	101.2	1.2
eu broken prism A [5]	3	462	0.42	1.3	1357	0.14001	0.00166	0.01949	0.00020	0.88	0.05210	0.00029	124.4	1.3	133.1	1.5
DZ05-6, tonalite (Zouluzar), Dehshir ophiolite (31°17'32"N, 53°53'67")																
eu tip CA [1]	1	157	0.29	2.1	92	0.1065	0.0102	0.01552	0.00011	0.68	0.04977	0.00455	99.3	0.7	102.8	9.3
eu long prism CA [1]	1	231	0.81	3.6	81	0.0971	0.0084	0.01549	0.00012	0.53	0.04546	0.00376	99.1	0.8	94.1	7.7
eu short prism A [1]	1	160	0.70	0.6	291	0.1077	0.0044	0.01538	0.00014	0.45	0.05079	0.00192	98.4	0.9	103.9	4.0
eu long clear tip CA [1]	1	184	0.28	0.7	259	0.1011	0.0037	0.01531	0.00006	0.53	0.04791	0.00164	98.0	0.4	97.8	3.4
eu tip A [1]	1	161	0.31	1.7	108	0.0987	0.0084	0.01498	0.00009	0.64	0.04779	0.00390	95.9	0.6	95.6	7.8

[1]eu, euhedral; fr, fragment; CA or A, treated with chemical abrasion or air abrasion; numbers in brackets indicate number of grains.
[2]Weight and concentrations are known to better than 10%, except for those near and below the *c*. 1 μg limit of resolution of the balance.
[3]Th/U model ratio inferred from 208/206 ratio and age of sample.
[4]Pbc is the total common Pb in sample (initial + blank).
[5]Raw data corrected for fractionation.
[6]Corrected for fractionation, spike, blank, initial common Pb and initial ^{230}Th disequilibrium (assuming Th/U magma = 4) ; error calculated by propagating the main sources of uncertainty.

lithophile elements (LILE) and depleted in high field strength elements (HFSE) relative to N-MORB, similar to island-arc tholeiites (Fig. 5b). Its REE and trace elements patterns are similar to those of Nain arc tholeiitic gabbros (Shafaii Moghadam 2008). The various models suggested for plagiogranite formation in ophiolitic complexes and/or oceanic crust (Juteau *et al*. 1988; Koepke *et al*. 2004) include fractional crystallization of basaltic melts, hydrous partial melting of gabbroic rocks and hydrous anatexis of an altered sheeted dyke complex. REE and trace element similarities between Nain plagiogranites and island-arc tholeiitic gabbros suggest that these plagiogranites are residual melts produced during fractional crystallization of tholeiitic gabbros, and thus can provide only a minimum constraint on the timing of ophiolite formation.

Zircon occurs mainly as broken euhedral prisms, with rare fully preserved crystals (Fig. 6) containing 403–594 ppm U and with Th/U ratios of 0.48–0.55 (Table 1). The four analyses define a mean $^{206}Pb/^{238}U$ age of 102.8 ± 0.3 Ma (Fig. 6). The high MSWD of 3.4 is caused by slight discordance of two analyses, possibly as a result of a xenocrystic component. Exclusion of these two points reduces the age to 102.7 ± 0.2 Ma, which we take as approximating that of Nain ophiolite formation.

Dehshir ophiolite: sample AZ06-25 (plagiogranite dyke)

Plagiogranite dykes in the Aziz-Abad diorite (including AZ06-24) are composed of altered plagioclase, quartz, orthoclase, amphibole and chlorite. The rock has a concave-up REE pattern with positive Eu anomaly, suggesting plagioclase accumulation (Fig. 5a). Depletion of Nb and Ta and LILE enrichment are characteristic of the dyke, indicating suprasubduction-zone affinity (Fig. 5b). The plagiogranite also has Sr/Y *c*. 60, similar to adakite, suggesting that these are anatectic melts of amphibolite (Shafaii Moghadam *et al*. 2010).

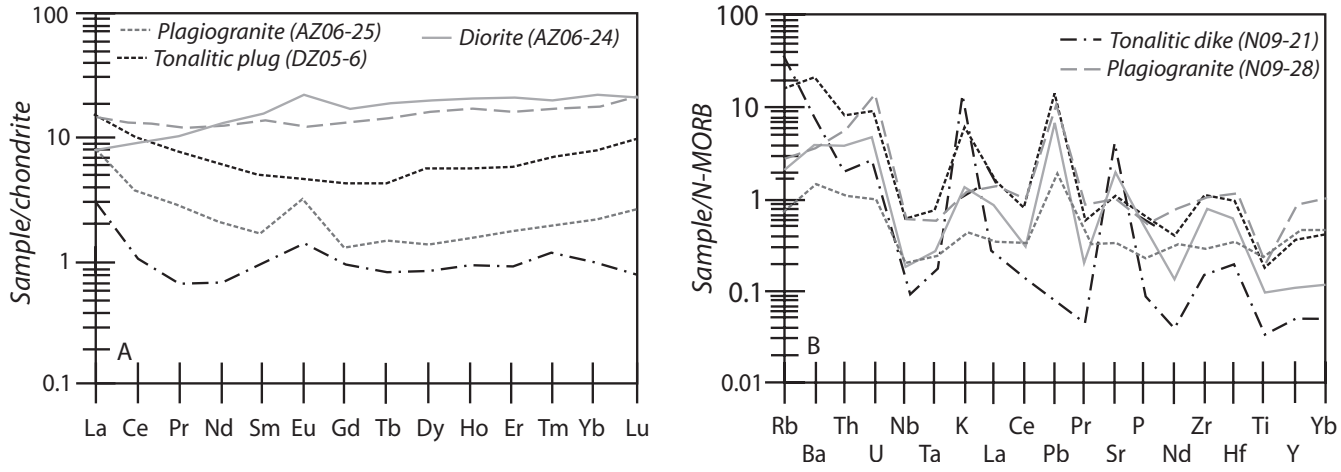

Fig. 5. (**a**) Chondrite-normalized REE patterns (chondrite abundances are from McDonough & Sun 1995) and (**b**) normal mid-ocean ridge basalt (N-MORB)-normalized multi-element patterns (N-MORB concentrations are from Sun & McDonough 1989) for dated rock units of Nain and Dehshir ophiolites. The whole-rock data for the Nain and Dehshir ophiolites are from Shafaii Moghadam (2008) and Shafaii Moghadam *et al*. (2010), respectively.

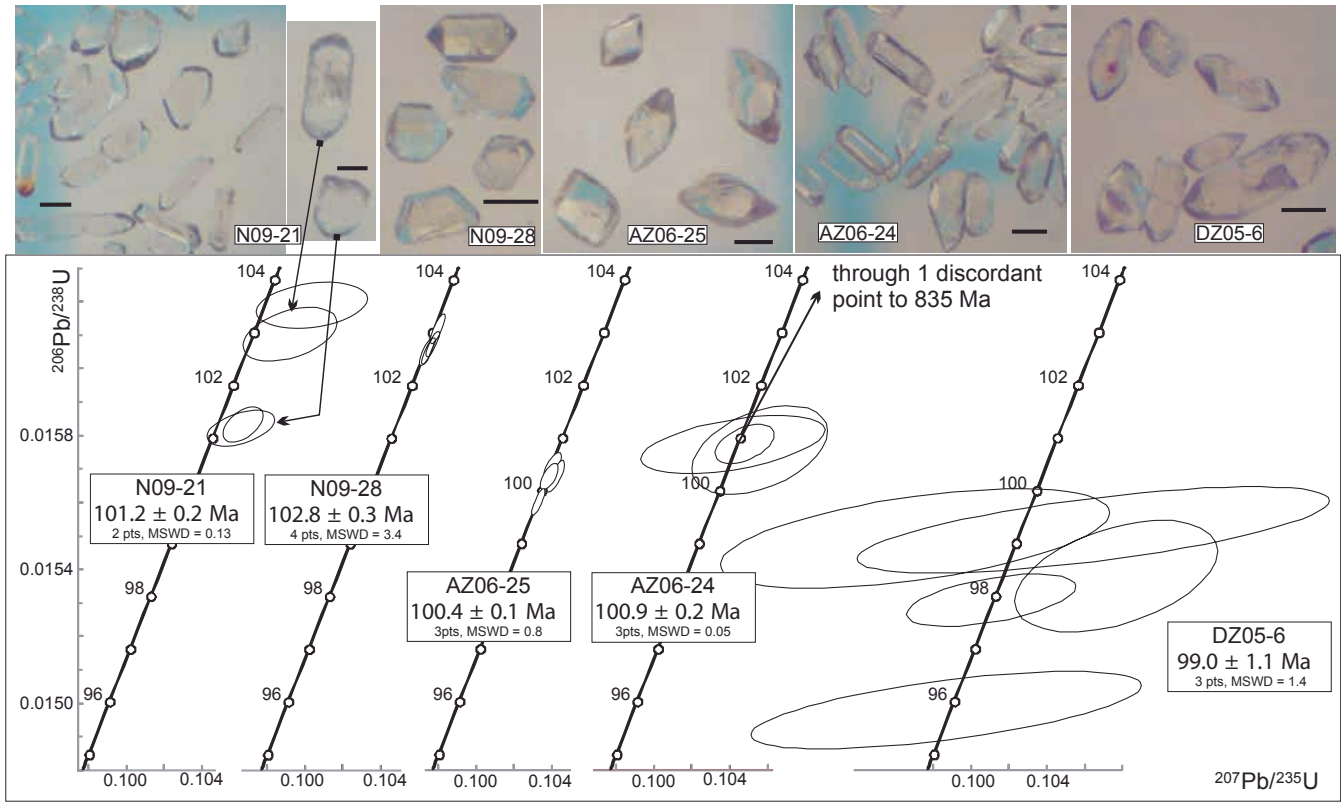

Fig. 6. Zircon photomicrographs and stacked concordia diagrams displaying U–Pb data from the Nain (N09-21 and 28) and Dehshir (AZ06-24 and 25, ZDZ05-6) ophiolites. Ellipses represent 2σ errors. The scale bar in the zircon images represents 100 μm.

The abundant zircon population consists of short prisms with prominent {211} pyramids (Fig. 6). Three analyses yield a mean $^{206}Pb/^{238}U$ age of 100.4 ± 0.1 Ma, whereas a fourth point is slightly younger, suggesting Pb loss. We take this age as approximating the age of formation of the Dehshir ophiolite.

Dehshir ophiolite: sample AZ06-24 (diorite)

Isotropic diorites with crosscutting plagiogranite dykes (including AZ06-25, above) crop out SW of Aziz-Abad village (Fig. 4c). These diorites are found as lenses with fault contacts with overlying pillow lavas. Plagioclase and amphibole (magnesio-hornblende) are the main rock-forming minerals. Plagioclase is altered to sericite and clays whereas amphiboles are altered to chlorite. The sample has a light REE (LREE)-depleted pattern with slight positive Eu anomaly (Fig. 5a). The diorite displays positive anomalies in Rb, Ba, U, Th and Pb and negative anomalies in Nb and Ta relative to N-MORB, indicating a suprasubduction-zone affinity (Fig. 5b).

The zircon population consists of a mix of long-prismatic and short-prismatic to euhedral crystals, commonly occurring as

broken fragments (Fig. 6). Three single grain analyses (Table 1) overlap on concordia giving a mean $^{206}Pb/^{238}U$ age of 100.9 ± 0.2 Ma. A multigrain fraction is discordant owing to a xenocrystic component, whose age is indicated by the projection of the data point (outside the field shown in Fig. 6) towards about 835 Ma. The older age with respect to the 100.4 ± 0.1 Ma plagiogranite is consistent with the observed crosscutting relationships. These diorites occur with the sheeted dyke complex (although contacts are faulted), and geochemically are similar to Dehshir crustal gabbros and lavas (see Shafaii Moghadam & Stern 2011), and so far we can take this age as approximating that of Dehshir ophiolite formation.

Dehshir ophiolite: sample DZ05-6 (tonalitic plug within metamorphosed lavas and their pyroclastic equivalents)

Small tonalitic plugs intrude ophiolitic metamorphosed rocks (metamorphosed basaltic lava flows and their pyroclastic equivalents) near Zoolouzar village (Fig. 4d). The rocks have been metamorphosed to greenschist facies. These ophiolitic metamorphic rocks have faulted contacts with serpentinites, harzburgites and crustal amphibole gabbros. Small tonalite veins are also injected into amphibole gabbros. Geochemically the metavolcanic rocks have an island-arc tholeiitic signature similar to the overlying pillow lavas and isotropic gabbros. The tonalitic rocks are mainly composed of plagioclase, quartz, amphibole, biotite and chlorite, with U-shaped REE patterns (Fig. 5a). Positive anomalies in Rb, Ba, Th, U, Pb, K, Zr and Hf as well as depletions in Nb–Ta–Ti indicate a suprasubduction-zone affinity (Fig. 5b). REE and trace element patterns of these tonalites suggest hydrous partial melting products of tholeiitic gabbros during ophiolite emplacement.

Sample DZ05-6 contains few colourless long and short euhedral prisms (Fig. 6). The analyses are not very precise because of the small sample size, and they also show discordance. Three analyses yield a mean $^{206}Pb/^{238}U$ age of 99.0 ± 1.1 Ma, which dates intrusion of the plug and thus constrains the age of ophiolite emplacement. The other two analyses are more discordant, probably as a result of Pb loss.

Discussion

These U–Pb zircon ages indicate that the Nain and Dehshir ophiolites formed *c*. 100 Ma, with Nain (102.9 ± 0.3 Ma) being *c*. 1 Ma older than Dehshir (100.9 ± 0.2 Ma; 100.4 ± 0.1 Ma), and that these ophiolites developed a metamorphic sole during emplacement soon after formation (Nain emplacement 101.2 ± 0.2 Ma; Dehshir emplacement 99.0 ± 1.1 Ma). One uncertainty is whether tonalitic dykes intruding Nain garnet amphibolites are related to Eocene magmatism (Urumieh–Dokhtar arc) or are parts of the Nain ophiolite, because they intrude only amphibolites but not other ophiolitic units, nor Upper Cretaceous pelagic sediments. The geochemical characteristics of the tonalitic dykes differ from those of younger, Eocene calc-alkaline granitic rocks of the Urumieh–Dokhtar magmatic arc, so we conclude that these dykes are part of the ophiolite. The 100–102 Ma U–Pb zircon ages of the Nain and Dehshir ophiolites (Fig. 7) are consistent with biostratigraphic ages no older than Cenomanian–Coniacian (99.6–89.3 Ma) of conformably overlying pelagic sediments above both Inner and Outer Belt ophiolites (Table 2). These U–Pb zircon ages are 3–10 Ma older than existing K–Ar and up to 16 Ma older than $^{40}Ar/^{39}Ar$ ages for Zagros ophiolites, as discussed further below. Nain–Baft (Inner Belt) amphibolites and hornblende ophiolitic gabbros yield K/Ar hornblende ages of 93.4 ± 3.6 and 93.8 ± 8.7 Ma, respectively (Shafaii Moghadam *et al*. 2009), whereas dolerite and hornblende gabbro of the Outer Belt Neyriz ophiolite yield $^{40}Ar/^{39}Ar$ hornblende ages of 85.9 ± 3.8 and 94.9 ± 7.6 Ma, respectively (Lanphere & Pamic 1983). $^{40}Ar/^{39}Ar$ ages of 92.1 ± 1.7, 93.2 ± 2.5 (Babaie *et al*. 2006) and 99.1 ± 1.7 Ma (Jannessary 2003) have been reported from Inner Belt Neyriz hornblende gabbros (Babaie *et al*. 2006). Given that the new U–Pb zircon ages are best interpreted as magmatic crystallization ages, the significance of K/Ar and $^{40}Ar/^{39}Ar$ ages for these rocks needs to be critically re-examined.

The U–Pb zircon ages for Zagros ophiolites are older than those from other LCOBSA localities, with crystallization ages of 92 Ma for the Troodos ophiolite on Cyprus (Mukasa & Ludden 1987) and 94.4–98 Ma for Oman (Tilton *et al*. 1981; Warren *et al*. 2005). The younger age (94.4 Ma) is thought to reflect younging of the ophiolite across strike (Warren *et al*. 2005). Recent U–Pb zircon dating of United Arab Emirates (UAE) ophiolites (northern parts of Semail ophiolite) from younger, late stage micro-gabbroic dykes (crosscutting ophiolite crustal section as well as mantle rocks) and associated tonalitic rocks have yielded concordia ages of 95.74 ± 0.32 to 96.40 ± 0.29 and 95.26 ± 0.31 Ma, respectively (Goodenough *et al*. 2010). These geochronological data indicate that crystallization of late magmatic rocks occurred along the length of the Oman ophiolites over a period of around 1.2 Ma between *c*. 96.40 and 95.26 Ma (Warren *et al*. 2005; Goodenough *et al*. 2010). The U–Pb zircon ages overlap with ^{40}Ar–^{39}Ar hornblende ages between 93.6 ± 0.5 and 96.3 ± 1.3 Ma from Oman trondhjemites and nearby gabbros, interpreted as formation ages (Hacker *et al*. 1997).

LCOBSA ophiolites were emplaced soon after sea-floor spreading ended. The longest time span between formation and emplacement is seen for the Troodos ophiolite, where metamorphic rocks have ^{40}Ar–^{39}Ar amphibole ages (75.7 ± 0.3 to 88.9 ± 0.8 Ma) that are as much as 16 Ma younger than U–Pb zircon ages. Similarly, Baer–Bassit in Syria gives ^{40}Ar–^{39}Ar ages of 71.7 ± 0.5 to 88.4 ± 0.4 Ma on hornblende of amphibolites (Chan *et al*. 2007). In contrast, only a few million years separate igneous activity and emplacement of the Semail ophiolite. Hornblendes from the amphibolites-facies metamorphic sole of the Semail ophiolite yields 92.6 ± 0.6 and 94.9 ± 0.5 Ma (Hacker 1994; Hacker & Gnos 1997; Hacker *et al*. 1997). This agrees with $^{40}Ar/^{39}Ar$ ages on hornblende from Oman metamorphic sole amphibolites and its associated melt segregations of 94.5 ± 0.28 and 94.5 ± 0.33 Ma, respectively (Warren *et al*., 2005). These ages are interpreted as dating cooling of the metamorphic sole after ophiolite emplacement. Muscovite ^{40}Ar–^{39}Ar dating yielded cooling ages between 90.9 and 93.4 ± 0.3 Ma for Semail metamorphic rocks (Gnos & Peters, 1993). Potassium–argon ages from Oman metamorphic rocks associated with the Semail ophiolite are 95–100 Ma (Montigny *et al*. 1988). Metamorphic rocks of the Tauride belt ophiolites of southern Turkey yield ^{40}Ar–^{39}Ar ages of 90.7 ± 0.5 to 93.9 ± 0.9 Ma for the Lycian ophiolite, 93.0 ± 1.0 to 93.8 ± 1.7 Ma for the Antalya ophiolite, 90.9 ± 1.3 to 91.5 ± 1.9 Ma for the Beysehir ophiolite, and 91.3 ± 0.4 to 96.0 ± 0.7 Ma for the Mersin ophiolite (Dilek *et al*. 1999; Parlak & Delaloye 1999; Celik *et al*. 2006).

The differences in U–Pb zircon ages between the Zagros and the other Eurasian ophiolites are consistent with differences in biostratigraphic ages for associated pelagic sediments. Coniacian–Cenomanian (99.6–89.3 Ma) pelagic sediments above Zagros ophiolites are slightly older than late Cenomanian–early Turonian (*c*. 93.5 Ma) limestone layers within Semail ophiolite volcanic rocks (with some overlap) and significantly older than Santonian (85.8–83.5 Ma) pelagic sediments on top of the Semail ophiolite (e.g. Robertson & Fleet 1986; Garfunkel 2006) (Table 2). This is also true for Turonian–Maastrichtian pelagic limestones above Troodos ophiolitic lavas. This supports the older U–Pb zircon ages of Zagros ophiolites and further suggests that subduction was first initiated at or near the Zagros margin and propagated to the east and west. Westward propagation rates of *c*. 15 cm a^{-1} (from Zagros to Cyprus) and eastward rates of *c*. 7 cm a^{-1} (from Zagros to Semail) can explain the observed U–Pb zircon ages (Fig. 7).

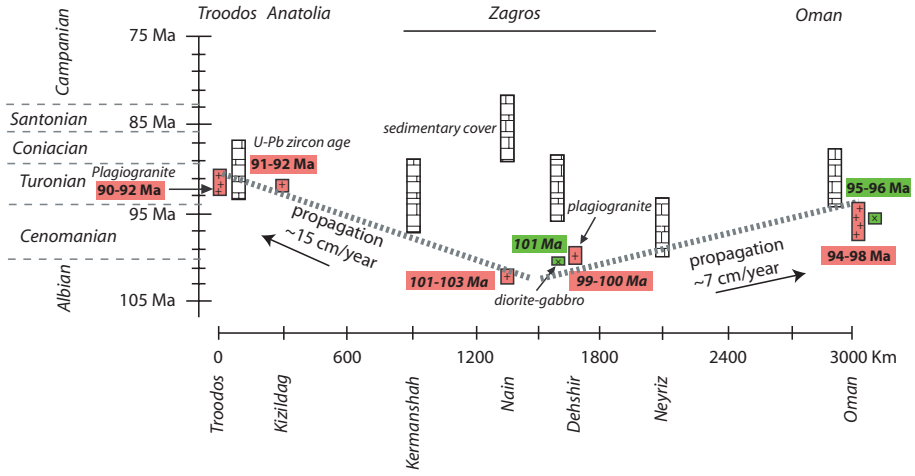

Fig. 7. Compilation of U–Pb zircon dating results for igneous rocks from the Late Cretaceous Neotethyan ophiolites along the 3000 km long Bitlis–Zagros suture zone. (For U–Pb age references see Table 2.) Biostratigraphic ages indicate the oldest reliable age for sediments either within or stratigraphically overlying the ophiolites.

Table 2. *Characteristics and ages of Late Cretaceous Tethyan ophiolites*

Age of overlying sediments (Ma)	Isotopic dating results (Ma)	Type of dated rock	Dating method	References
Troodos				
Turonian–Maastrichtian	92	Plagiogranite	Zircon U–Pb TIMS	Mukasa & Ludden 1987
(93.5–65.5)	76–89	Metamorphic sole	Amphibole Ar–Ar	Chan *et al*. 2007
Kizildag				
Maastrichtian (65.5)	91–92	Plagiogranite	Zircon U–Pb TIMS	Dilek & Thy 2009
Kermanshah (OB)				
Turonian–Maastrichtian (93.5–65.5)	83–86	Doleritic dyke	Amphibole K–Ar	Delaloye & Desmons 1980
Neyriz (OB)				
Cenomanian–Turonian	92–93	Amphibole gabbro	Amphibole Ar–Ar	Babaie *et al*. 2006
to Early Santonian	86–93	Amphibole gabbro	Amphibole Ar–Ar	Lanphere & Pamic 1983
(99.6 to 89.3–85.8)	99	Amphibole gabbro	Amphibole Ar–Ar	Jannessary 2003
Nain (IB)				
Coniacian–Maastrichtian	93	Amphibole gabbro	Amphibole K–Ar	Shafaii Moghadam *et al*. 2009
(89.3–65.5)	101–102	Plagiogranite	Zircon U–Pb TIMS	This study
Dehshir (IB)				
Turonian–Maastrichtian	67–94	Amphibole gabbro	Amphibole K–Ar	Shafaii Moghadam *et al*. 2009
(93.5–65.5)	99–100	Plagiogranite	Zircon U–Pb TIMS	This study
Balvard–Baft (IB)				
Turonian–Maastrichtian (93.5–65.5)	72–94	Amphibole gabbro	Amphibole K–Ar	Shafaii Moghadam *et al*. 2009
Oman				
Late Cenomanian–Early Turonian	93–98	Plagiogranite	Zircon U–Pb TIMS	Tilton *et al*. 1981
to Early Santonian	96–95	Gabbroic and tonalitic rocks	Zircon U–Pb TIMS	Goodenough *et al*. 2010
(93.5–85.8)	96–94	Trondhjemite	Zircon U–Pb TIMS	Warren *et al*. 2005
	92–95	Metamorphic sole	Amphibole Ar–Ar	Hacker *et al*. 1997
	93–96	Trondhjemite and gabbro	Amphibole Ar–Ar	Hacker *et al*. 1997
	94	Amphibolite and felsic segregations	Zircon U–Pb TIMS	Warren *et al*. 2005

More U–Pb zircon ages for Zagros ophiolites are needed to test the idea that a new subduction zone began in Late Cretaceous time on the SW margin of Eurasia and to constrain the rate at which subduction initiation propagated along this margin. We especially need U–Pb zircon ages for Zagros Outer Belt ophiolites to test the idea that the two Zagros belts were once parts of a single coherent forearc lithosphere. We also need to understand how Zagros forearc igneous activity related to subduction initiation evolved into the mature magmatic arc now represented by the Urumieh–Dokhtar arc. Radiometric ages for igneous rocks of this arc are rare but recent studies yield a Rb–Sr isochron age of 33 ± 1 Ma for arc granitic rocks (Dargahi *et al*. 2010). The presence of pyroclastic rocks associated with Late Cretaceous pelagic sediments just above the Balvard–Baft ophiolite (southernmost ophiolite of the Inner Belt), along with the observation that these pyroclastic rocks thicken to the NE, suggests that an arc like the Urumieh–Dokhtar magmatic arc existed in Late Cretaceous time (Shafaii Moghadam & Stern 2011). These observations further indicate that the Urumieh–Dokhtar magmatic arc can be interpreted as the arc that formed following Late Cretaceous subduction initiation as discussed above.

Conclusions

New U–Pb zircon geochronological data for Nain and Dehshir ophiolites (Zagros Inner Belt ophiolites) provide new insights on the timing of Late Cretaceous subduction initiation to generate ophiolites along the Zagros–Bitlis suture zone. Our results indicate that Zagros ophiolites are significantly older than other ophiolites along this suture. Consequently, a diachronous tectonic evolution for Neotethyan ophiolites along the SW Eurasian margin has to be considered, whereby subduction began near present-day Iran and propagated from there to the east and west.

We are very grateful to C.J. Warren, M. Santosh and K. Goodenough for their constructive reviews of the manuscript. Editorial suggestions by Dr. Quentin G. Crowley are highly appreciated. We are most thankful to the Damghan University for logistical support during field work. This is UTD Geosciences Contribution #1235.

References

Agard, P., Monie, P., *et al*. 2006. Transient, synobduction exhumation of Zagros blueschists inferred from *P–T*, deformation, time, and kinematic constraints: implications for Neo-Tethyan wedge dynamics. *Journal of Geophysical Research*, **111**, doi:10.1029/2005JB004103.

Agard, P., Omrani, J., *et al*. 2011. Zagros Orogeny: a subduction-dominated process. *Geological Magazine*, **148**, 692–725.

Alabaster, T., Pearce, J.A. & Malpas, J. 1982. The volcanic stratigraphy and petrogenesis of the Oman ophiolite. *Contributions to Mineralogy and Petrology*, **81**, 168–183.

Alavi, M. 1994. Tectonics of the Zagros orogenic belt of Iran: new data and interpretations. *Tectonophysics*, **229**, 211–238.

Alavi, M. 2007. Structures of the Zagros fold–thrust belt in Iran. *American Journal of Science*, **307**, 1064–1095, doi:10.2475/09.2007.02.

Arai, S., Kadoshima, K. & Morishita, T. 2006. Widespread arc-related melting in the mantle section of the northern Oman ophiolite as inferred from detrital chromian spinels. *Journal of the Geological Society, London*, **163**, 869–879.

Babaie, H.A., Babaei, A., Ghazi, A.M. & Arvin, M. 2006. Geochemical, $^{40}Ar/^{39}Ar$ age, and isotopic data for crustal rocks of the Neyriz ophiolite, Iran. *Canadian Journal of Earth Sciences*, **43**, 57–70.

Bagci, U. & Parlak, O. 2009. Petrology of the Tekirova (Antalya) ophiolite (Southern Turkey): evidence for diverse magma generations and their tectonic implications during Neotethyan subduction. *International Journal of Earth Sciences*, **98**, 387–405.

Bagci, U., Parlak, O. & Hock, V. 2005. Whole rock and mineral chemistry of cumulates from the Kızıldag (Hatay) ophiolite (Turkey): clues for multiple magma generation during crustal accretion in the southern Neotethyan Ocean. *Mineralogical Magazine*, **69**, 53–76.

Bagci, U., Parlak, O. & Hock, V. 2006. Geochemical character and tectonic environment of ultramafic to mafic cumulates from the Tekirova (Antalya) ophiolite (Southern Turkey). *Geological Journal*, **41**, 193–219.

Bagci, U., Parlak, O. & Hock, V. 2008. Geochemistry and tectonic environment of diverse magma generations forming the crustal units of the Kizildag (Hatay) ophiolite, southern Turkey. *Turkish Journal of Earth Sciences*, **17**, 43–71.

Berberian, F. & Berberian, M. 1981. Tectono-plutonic episodes in Iran. *In*: Gupta, H.K. & Delany, F.M. (eds) *Zagros, Hindukush, Himalaya Geodynamic Evolution*. American Geophysical Union, Geodynamics Series, **3**, 5–32.

Berberian, M. & King, G.C.P. 1981. Towards a paleogeography and tectonic evolution of Iran. *Canadian Journal of Earth Science*, **18**, 210–265.

Berberian, F., Muir, I.D., Pankhurst, R.J. & Berberian, M. 1982. Late Cretaceous and early Miocene Andean type plutonic activity in northern Makran and Central Iran. *Journal of the Geological Society, London*, **139**, 605–614.

Celik, O.F., Delaloye, M. & Feraud, G. 2006. Precise $^{40}Ar–^{39}Ar$ ages from the metamorphic sole rocks of the Tauride Belt ophiolites, southern Turkey: implications for the rapid cooling history. *Geological Magazine*, **143**, 213–227.

Chan, G.H.-N., Malpas, J. & Xenophontos, C. 2007. Timing of subduction zone metamorphism during the formation and emplacement of Troodos and Baer–Bassit ophiolites: insights from $^{40}Ar–^{39}Ar$ geochronology. *Geological Magazine*, **144**, 797–810.

Coleman, R.G. 1984. The diversity of ophiolites. *Geologie en Mijnbouw*, **63**, 141–150.

Corfu, F. 2004. U–Pb age, setting, and tectonic significance of the anorthosite–mangerite–charnockite–granite-suite, Lofoten–Vesterålen, Norway. *Journal of Petrology*, **45**, 1799–1819.

Dargahi, S., Arvin, M., Pan, Y. & Babaei, A. 2010. Petrogenesis of post-collisional A-type granitoids from the Urumieh–Dokhtar magmatic assemblage, southwestern Kerman: constraints on the Arabian–Eurasian continental collision. *Lithos*, **115**, 190–204.

Davies, G.F. 1999. *Dynamic Earth*. Cambridge University Press, New York.

Davoudzadeh, M. 1972. *Geology and Petrography of the Area North of Nain, Central Iran*. Geological Survey of Iran, Report, **14**.

Delaloye, M. & Desmons, J. 1980. Ophiolites and mélange terranes in Iran: a geochronological study and its paleotectonic implications. *Tectonophysics*, **68**, 83–111.

Dilek, Y. & Flower, M.F.J. 2003. Arc–trench rollback and forearc accretion: a model template for ophiolites in Albania, Cyprus and Oman. *In*: Dilek, Y. & Robinson, P.T. (eds) *Ophiolites in Earth History*. Geological Society, London, Special Publications, **218**, 43–48.

Dilek, Y. & Furnes, H. 2011. Ophiolite genesis and global tectonics: tectonic fingerprinting of ancient oceanic lithosphere. *Geological Society of America Bulletin*, **123**, 387–411.

Dilek, Y. & Thy, P. 2009. Island arc tholeiite to boninitic melt evolution of the Cretaceous Kizildag (Turkey) ophiolite: model for multi-stage early arc–forearc magmatism in Tethyan subduction factories. *Lithos*, **113**, 68–87.

Dilek, Y., Thy, P., Hacker, B. & Grundvig, S. 1999. Structure and petrology of Tauride ophiolites and mafic dyke intrusions (Turkey): implications for the Neotethyan ocean. *Geological Society of America Bulletin*, **111**, 1192–1216.

Dilek, Y., Furnes, H. & Shallo, M. 2007. Suprasubduction zone ophiolite formation along the periphery of Mesozoic Gondwana. *Gondwana Research*, **11**, 453–475.

Elthon, D. 1991. Geochemical evidence for the Bay of Islands ophiolite above a subduction zone. *Nature*, **354**, 140–142.

Falcon, N.L. 1974. An outline of the geology of the Iranian Makran. *Geographical Journal*, **140**, 283–291.

Floyd, P.A., Yaliniz, M.K. & Goncuoglu, M.C. 1998. Geochemistry and petrogenesis of intrusive and extrusive ophiolitic plagiogranites, Central Anatolian Crystalline Complex, Turkey. *Lithos*, **42**, 225–241.

Garfunkel, Z. 2006. Neotethyan ophiolites: formation and obduction within the life cycle of the host basins. *In*: Robertson, A.H.F. & Mountrakis, D. (eds) *Tectonic Development of the Eastern Mediterranean Region*. Geological Society, London, Special Publications, **260**, 301–326.

Gerya, T. 2011. Future directions in subduction modeling. *Journal of Geodynamics*, **52**, 344–378.

Gnos, E. & Peters, T. 1993. K–Ar ages of the metamorphic sole of the Semail ophiolites: implications for ophiolite cooling history. *Contributions to Mineralogy and Petrology*, **113**, 325–332.

Godard, M., Dautria, J.M. & Perrin, M. 2003. Geochemical variability of the Oman ophiolite lavas: relationship with spatial distribution and paleomagnetic directions. *Geochemistry, Geophysics, Geosystems*, **4**, doi:10.1029/2002GC000452.

Godard, M., Bosch, D. & Einaudi, F. 2006. A MORB source for low-Ti magmatism in the Semail ophiolite. *Chemical Geology*, **234**, 58–78.

Goodenough, K.M., Style, M.T., *et al*. 2010. Architecture of the Oman–UAE ophiolite: evidence for a multi-phase magmatic history. *Arabian Journal of Geosciences*, **3**, 439–458.

Hacker, B.R. 1994. Rapid emplacement of young oceanic lithosphere: argon geochronology of the Oman ophiolite. *Science*, **265**, 1563–1565.

Hacker, B.R. & Gnos, E. 1997. The conundrum of Semail: explaining the metamorphic history. *Tectonophysics*, **279**, 215–226.

Hacker, B.R., Mosenfelder, J.L. & Gnos, E. 1997. Rapid emplacement of the Oman ophiolite: thermal and geochronologic constraints. *Tectonics*, **15**, 1230–1247.

Hébert, R. & Laurent, R. 1990. Mineral chemistry of the plutonic section of the Troodos ophiolite: new constraints for genesis of arc-related ophiolites. *In*: Malpas, J., Moores, E., Panayiotou, A. & Xenophontos, C. (eds) *Ophiolites: Oceanic Crustal Analogues. Proceedings of the Symposium 'Troodos 1987'*. Geological Survey Department, Nicosia, 149–163.

Hebert, R., Bezard, R., Guilmette, C., Dostal, J., Wang, C.S. & Liu, Z.F. 2012. The Indus–Yarlung Zangbo ophiolites from Nanga Parbat to Namche Barwa syntaxes, southern Tibet: first synthesis of petrology, geochemistry and geochronology with incidences on geodynamic reconstructions of Neo-Tethys. *Gondwana Research* **22**, 377–397, http://dx.doi.org/10.1016/j.gr.2011.10.013.

Ishizuka, O., Tani, K., *et al*. 2011. The timescales of subduction initiation and subsequent evolution of an oceanic island arc. *Earth and Planetary Science Letters*, **306**, 229–240.

Jaffey, A.H., Flynn, K.F., Glendenin, L.E., Bentley, W.C. & Essling, A.M. 1971. Precision measurement of halflives and specific activities of ^{235}U and ^{238}U. *Physical Review C: Nuclear Physics*, **4**, 1889–1906.

Jannessary, M.R. 2003. Les ophiolites de Neyriz (sud de l'Iran): naissance d'une dorsale en pied de marge continentale (étude des structures internes, de la fabrique du manteau, et de l'évolution petro-géochimique des magmas). Unpublished PhD thesis, Université de Louis Pasteur, Strasbourg.

Juteau, T., Ernewein, M., Reuber, I., Whitechurch, H. & Dahl, R. 1988. Duality of magmatism in the the plutonic sequence of the Semail nappe, Oman. *Tectonophysics*, **151**, 107–136.

Koepke, J., Feig, S.T., Snow, J. & Freise, M. 2004 Petrogenesis of oceanic plagiogranites by partial melting of gabbros: an experimental

study. *Contributions to Mineralogy and Petrology*, **146**, 414-432, http://dx.doi.org/10.1007/s00410-003-0511-9

Krogh, T.E. 1973. A low contamination method for hydrothermal decomposition and extraction of U and Pb for isotopic age determinations. *Geochimica et Cosmochimica Acta*, **37**, 485–494.

Krogh, T.E. 1982. Improved accuracy of U/Pb zircon ages by creation of more concordant systems using air abrasion technique. *Geochimica et Cosmochimica Acta*, **46**, 637–649.

Lanphere, M.A. & Pamic, T. 1983. $^{40}Ar/^{39}Ar$ ages and tectonic setting of ophiolites from Neyriz area, south-east Zagros range, Iran. *Tectonophysics*, **96**, 245–256.

Leng, W. & Gurnis, M. 2011. Dynamics of subduction initiation with different evolutionary pathways. *Geochemistry, Geophysics, Geosystems*, **12**, doi:10.1029/2011GC003877.

Ludwig, K.R. 2003. *Isoplot 3.0: A Geochronological Toolkit for Microsoft Excel*. Berkeley Geochronological Center, Special Publications, **4**.

Lytwyn, J.N. & Casey, J.F. 1993. The geochemistry and petrogenesis of volcanics and sheeted dikes from the Hatay (Kızıldağ) ophiolite, southern Turkey: possible formation with the Troodos ophiolite, Cyprus, along fore-arc spreading centers. *Tectonophysics*, **232**, 237–272.

Mattinson, J.M. 2005. Zircon U–Pb chemical abrasion ('CA-TIMS') method: combined annealing and multi-step partial dissolution analysis for improved precision and accuracy of zircons ages. *Chemical Geology*, **220**, 47–66.

McDonough, W.F. & Sun, S.S. 1995. The composition of the Earth. *Chemical Geology*, **120**, 223–253.

Miyashiro, A. 1975. Classification, characteristics and origin of ophiolites. *Journal of Geology*, **83**, 249–281.

Montigny, R., Le Mer, O., Thuizat, R. & Whitechurch, H. 1988. K–Ar and $^{40}Ar/^{39}Ar$ study of the metamorphic rocks associated with the Oman ophiolite. *Tectonophysics*, **151**, 345–362.

Mukasa, S. & Ludden, J.N. 1987. Uranium–lead isotopic ages of plagiogranites from the Troodos ophiolite, Cyprus, and their tectonic significance. *Geology*, **15**, 825–828.

Parlak, O. & Delaloye, M. 1999. Precise $^{40}Ar–^{39}Ar$ ages from the metamorphic sole of the Mersin ophiolite (Southern Turkey). *Tectonophysics*, **301**, 145–158.

Parlak, O., Delaloye, M. & Bingöl, E. 1996. Mineral chemistry of ultramafic and mafic cumulates as an indicator of the arc-related origin of the Mersin ophiolite (southern Turkey). *Geologische Rundschau*, **85**, 647–661.

Parlak, O., Hock, V. & Delaloye, M. 2000. Suprasubduction zone origin of the Pozanti–Karsanti ophiolite (southern Turkey) deduced from whole-rock and mineral chemistry of the gabbroic cumulates. *In*: Bozkurt, E., Winchester, J.A. & Piper, J.D.A. (eds) *Tectonics and Magmatism in Turkey and the Surrounding Area*. Geological Society, London, Special Publications, **173**, 219–234.

Parlak, O., Hock, V., Kozlu, H. & Delaloye, M. 2004. Oceanic crust generation in an island arc tectonic setting, SE Anatolian Orogenic Belt (Turkey). *Geological Magazine*, **141**, 583–603.

Parlak, O., Rizaoğlu, T., Bağcı, U., Karaoğlan, F. & Höck, V. 2009. Tectonic significance of the geochemistry and petrology of ophiolites in southeast Anatolia, Turkey. *Tectonophysics*, **473**, 173–187.

Pearce, J.A. 2003. Supra-subduction zone ophiolites: the search for modern analogues. *In*: Dilek, Y. & Newcomb, S. (eds) *Ophiolite Concept and the Evolution of Geological Thought*. Geological Society of America, Special Papers, **373**, 269–293.

Pearce, J.A. & Robinson, P.T. 2010. The Troodos ophiolitic complex probably formed in a subduction initiation, slab edge setting. *Gondwana Research*, **18**, 60–81.

Python, M., Ceuleneer, G. & Arai, S. 2008. Chromian spinels in mafic–ultramafic mantle dykes: evidence for a two-stage melt production during the evolution of the Oman ophiolite. *Lithos*, **106**, 137–154.

Rahmani, F., Noghreyan, M. & Khalili, M. 2007. Geochemistry of sheeted dikes in the Nain ophiolite (Central Iran). *Ofioliti*, **32**, 119–129.

Reagan, M.K., Ishizuka, O., *et al.* 2010. Fore-arc basalts and subduction initiation in the Izu–Bonin–Mariana system. *Geochemistry, Geophysics, Geosystems*, **11**, doi:10.1029/2009GC002871.

Robertson, A.H.F. 1998. Mesozoic–Tertiary tectonic evolution of the easternmost Mediteranean area: integration of marine and land evidence. *In*: Robertson, A.H.F., Emeis, K.C. & Camerlenghi, A. (eds) *Proceeding of the Ocean Drilling Program, Scientific Results, 160*. Ocean Drilling Program, College Station, TX, 723–782.

Robertson, A.H.F. 2002. Overview of the genesis and emplacement of Mesozoic ophiolites in the Eastern Mediterranean Tethyan region. *Lithos*, **65**, 10–67.

Robertson, A.H.F. & Fleet, A.J. 1986. Geochemistry and palaeo-oceanography of metalliferous and pelagic sediments from the Late Cretaceous Oman ophiolite. *Marine and Petroleum Geology*, **3**, 315–337.

Robertson, A.H.F. & Mountrakis, D. 2006. Tectonic development of the Eastern Mediterranean region: an introduction. *In*: Robertson, A.H.F. & Mountrakis, D. (eds) *Tectonic Development of the Eastern Mediterranean Region*. Geological Society, London, Special Publications, **260**, 1–9.

Schärer, U. 1984. The effect of initial ^{230}Th disequilibrium on young U–Pb ages: the Makalu case, Himalaya. *Earth and Planetary Science Letters*, **67**, 191–204.

Schoene, B., Crowley, J.L., Condon, D.C., Schmitz, M.D. & Bowring, S.A. 2006. Reassessing the uranium decay constants for geochronology using ID-TIMS U–Pb data. *Geochimica et Cosmochimica Acta*, **70**, 426–445.

Sengor, A.M.C. 1990. A new model for the late Paleozoic–Mesozoic tectonic evolution of Iran and implications for Oman. *In*: Robertson, A.H.F., Searle, M.P. & Ries, A.C. (eds) *The Geology and Tectonics of the Oman Region*. Geological Society, London, Special Publications, **49**, 797–831.

Shafaii Moghadam, H. 2008. *Nain-Baft ophiolitic belt: Age, Structure and Origin*. Unpublished PhD thesis, Shahid Beheshti University, Tehran, Iran.

Shafaii Moghadam, H. & Stern, R.J. 2011. Geodynamic evolution of late Cretaceous Zagros ophiolites: formation of oceanic lithosphere above a nascent subduction zone. *Geological Magazine*, **148**, 762–801.

Shafaii Moghadam, H., Whitechurch, H., Rahgoshay, M. & Monsef, I. 2009. Significance of Nain–Baft ophiolitic belt (Iran): short-lived, transtensional Cretaceous back-arc oceanic basins over the Tethyan subduction zone. *Comptes Rendus Geoscience*, **341**, 1016–1028.

Shafaii Moghadam, H., Stern, R.J. & Rahgoshay, M. 2010. The Dehshir ophiolite (central Iran): geochemical constraints on the origin and evolution of the Inner Zagros ophiolite Belt. *Geological Society of America Bulletin*, **122**, 1516–1547.

Shahabpour, J. 2007. Island-arc affinity of the Central Iranian Volcanic Belt. *Journal of Asian Earth Sciences*, **30**, 652–665.

Shervais, J.W. 2001. Birth, death and resurrection: the life cycle of suprasubduction zone ophiolites. *Geochemistry, Geophysics, Geosystems*, **2**, doi:10.109/2000GC000080.

Stern, R.J. 2004. Subduction initiation: spontaneous and induced. *Earth and Planetary Science Letters*, **226**, 275–292.

Stern, R.J., Reagan, M., Ishizuka, O., Ohara, Y. & Whattam, S. 2012. To understand subduction initiation, study forearc crust; to understand forearc crust, study ophiolites. *Lithosphere*, doi:10.1130/L183.1.

Stocklin, J. 1977. Structural correlation of the Alpine range between Iran and Central Asia. *Mémoire Hors-Série, Société Géologie de la France*, **8**, 333–353.

Sun, S.S. & McDonough, W.F. 1989. Chemical and isotopic systematics of oceanic basalts: implications for mantle composition and processes. *In*: Saunders, A.D. & Norry, M.J. (eds) *Magmatism in the Ocean Basins*. Geological Society, London, Special Publications, **42**, 313–345.

Tilton, G.R., Hopson, C.A. & Wright, J.E. 1981. Uranium–lead isotopic ages of the Semail Ophiolite, Oman, with applications to Tethyan ridge tectonics. *Journal of Geophysical Research*, **86**, 2763–2775.

Umino, S., Yanai, S., Jaman, A.R., Nakamura, Y. & Iiyama, J.T. 1990. The transition from spreading to subduction: evidence from the Semail ophiolite, northern Oman Mountains. *In*: Malpas, J., Moores, E.M., Panayiotou, A. & Xenophontos, C. (eds) *Ophiolites: Oceanic Crustal Analogues. Proceedings of the Symposium 'Troodos 1987'*. Geological Survey Department, Nicosia, 375–395.

Uysal, I., Ersoy, E.Y., *et al.* 2012. Coexistence of abyssal and ultra-depleted SSZ type mantle peridotites in a Neo-Tethyan ophiolite in SW Turkey: constraints from mineral composition, whole rock geochemistry (major–trace–REE–PGE) and Re–Os isotope systematic. *Lithos*, **132–133**, 50–69.

Vlaar, N.J. & Wortel, M.J.R. 1976. Lithospheric aging, instability and subduction. *Tectonophysics*, **32**, 331–351.

Warren, C.J., Parrish, R.R., Waters, D.J. & Searle, M.P. 2005. Dating the geologic history of Oman's Semail ophiolite: insights from U–Pb geochronology. *Contributions to Mineralogy and Petrology*, **150**, 403–422.

Whattam, S.A. & Stern, R.J. 2011. The 'subduction initiation rule': a key for linking ophiolites, intra-oceanic forearcs, and subduction initiation. *Contributions to Mineralogy and Petrology*, doi:10.1007/s00410-011-0638-z.

Yaliniz, K.M., Floyd, P. & Goncuoglu, M.C. 1996. Supra-subduction zone ophiolites of central Anatolia: geochemical evidence from the Sarikaraman ophiolite, Aksaray, Turkey. *Mineralogical Magazine*, **60**, 697–710.

Yamasaki, T., Maeda, J. & Mizuta, T. 2006. Geochemical evidence in clinopyroxenes gabbroic sequence for two distinct magmatism in the Oman ophiolite. *Earth and Planetary Science Letters*, **251**, 52–65.

Yilmaz, Y. 1993. New evidence and model on the evolution of the southeast Anatolian Orogen. *Geological Society of America Bulletin*, **105**, 251–271.

Yilmaz, Y., Yiğitbaş, E. & Genç, Ş.C. 1993. Ophiolitic and metamorphic assemblages of southeast Anatolia and their significance in the geological evolution of the orogenic belt. *Tectonics*, **12**, 1280–1297.

Received 21 May 2012; revised typescript accepted 9 July 2012.
Scientific editing by Quentin Crowley.